Relating nuclear magnetic resonance relaxation time distributions to void-size distributions for unconsolidated sand packs

Kristina Keating[1] and Samuel Falzone[1]

ABSTRACT

Nuclear magnetic resonance (NMR) is used in near-surface geophysics to understand the pore-scale properties of geologic material. The interpretation of NMR data in geologic material assumes that the NMR relaxation time distribution (T_2-distribution) is a linear transformation of the void-size distribution (VSD). This interpretation assumes fast diffusion and can be violated for materials with high surface relaxivity and/or large pores. We compared T_2-distributions to VSDs using grain-size distributions (GSDs) as a proxy for VSDs. Measurements were collected on water-saturated sand packs with a range of grain sizes and surface relaxivities, such that some samples were expected to violate the fast diffusion assumption. Samples were prepared from silica sand with three different average grain sizes and were coated with the iron-oxide mineral hematite to vary the surface relaxivity. We found analytically that outside the fast diffusion regime, the T_2-distributions are broader than in the fast diffusion regime, which could lead to misinterpretation of NMR data. The experimental results showed that the T_2-distributions were not linear transformations of the GSDs. The GSDs were a single peak independent of the hematite coating. The T_2-distributions were broader than the measured GSDs, and the center of the distribution depended on the coating. Using an equation that does not assume fast diffusion to transform the T_2-distributions to NMR-estimated VSDs resulted in distributions that were centered on a single radius. However, our attempts to recover the VSDs, as estimated from laser particle size analysis, were unsuccessful; the NMR-estimated VSDs were broader and yielded average pore radii that were much smaller than expected. We found that our approach was useful for determining relative VSDs from T_2-distributions; however, future research is needed to develop a method for calibrating the NMR-estimated VSDs for unconsolidated sands.

INTRODUCTION

The proton nuclear magnetic resonance (NMR) relaxation measurement is commonly used in the earth sciences to probe the pore-scale physiochemical environment of geologic material. Since the 1960s, NMR well-logging instruments have been used for the evaluation of petroleum reservoirs to detect hydrocarbon and water content and to estimate reservoir properties governing fluid flow, i.e., porosity, pore-size distribution, and permeability (Kleinberg, 1994; Allen et al., 2000). Recent developments of multichannel surface-based NMR instruments and borehole instruments designed to investigate near-surface sediments have led to an increase in the use of NMR for the evaluation of groundwater aquifers to determine water content, water-filled porosity, pore-size distribution, and hydraulic conductivity (Legchenko et al., 2004; Walsh et al., 2010; Dlugosch et al., 2011). Laboratory studies are commonly used to evaluate the NMR properties of geologic material, to improve the interpretation of NMR data, and to explore new applications (Kleinberg, 1994; Schaumann et al., 2005; Keating and Knight, 2007; Swanson et al., 2012). Improving the interpretation of NMR measurements for near-surface investigations is the application of interest in our research.

In water-saturated geologic material, the measured NMR signal is a multiexponential decay of magnetization characterized by an initial signal magnitude and a distribution of relaxation times or T_2-distribution. The initial signal magnitude is proportional to the number of protons in water and can be used to determine the volume of water in the measured sample. To date, near-surface NMR investigations have been primarily focused on the interpretation of NMR in water-saturated geologic material, in which case,

the initial signal magnitude is proportional to the water-filled porosity, and it is generally thought that the T_2-distribution is related to the pore geometry, specifically, that the T_2-distribution is a linear transformation of the pore or void size distribution (VSD) (e.g., Hinedi et al., 1993). The constant of proportionality linking the T_2-distribution to the VSD is the inverse of the surface relaxivity ρ_2, which is a measure of the ability of a surface to enhance relaxation. If ρ_2 is known or can be estimated, the T_2-distribution can be used to determine the VSD; it is this relationship that allows the NMR measurement to be used to estimate the permeability or hydraulic conductivity in geologic material via a Kozeny-Carman-type equation (e.g., Weller et al., 2010). The relationship between the T_2-distribution and the VSD has also led to recent interest in using NMR measurements to estimate parameters affecting contaminant transport (Swanson et al., 2012) and parameters governing the flow of water in the unsaturated zone, e.g., the characteristic water-retention curve (Bird et al., 2005; Costabel and Yaramanci, 2011a, 2011b, 2013).

A large body of literature comparing the T_2-distributions to VSDs or grain-size distributions (GSDs) has shown that the linear transformation holds for a range of water-saturated porous media including sandstone and carbonate rocks (Straley et al., 1997; Arns, 2004), silica gels (Valckenborg et al., 2001), fused glass beads (Straley et al., 1987), and unconsolidated sands and glass beads (Hinedi et al., 1993; Bird et al., 2005). These studies used materials in which the pore sizes were small and/or ρ_2 was low. However, the linear relationship relies on the assumption of fast diffusion, i.e., that protons can move to and interact with the surface of a pore within the time scale of the NMR experiment. For consolidated materials with small pores and/or for materials with low values of ρ_2, the assumption of fast diffusion is valid; however, for unconsolidated materials with large pores, e.g., coarse grains, and/or for materials with high values of ρ_2, the assumption of fast diffusion can be violated (Brownstein and Tarr, 1979). In this case, the T_2-distribution is not a linear transformation of the VSD. Recent works have shown that water-saturated sands with high ρ_2 have broader T_2-distributions than materials with low ρ_2 despite having similar grain sizes (Keating and Knight, 2007; Grunewald and Knight, 2011); however, to the best of our knowledge, no study has been published that systematically explores the relationship between the T_2-distribution and VSD for materials with high ρ_2 and large pores.

In this work, we conducted laboratory experiments designed to explore the effect of ρ_2 on the relationship between the T_2-distribution and the VSD in water-saturated sand packs. We are interested in understanding how violating the assumption of fast diffusion affects the T_2-distribution and so focus on materials with large pores, i.e., fine to coarse sands. To obtain measurements across samples with a range of VSDs, we used three sands with different GSDs. The GSD of a sand pack is expected to represent the VSD via a linear transformation or a modified version of the nonlinear Arya and Paris model (e.g., Arya and Paris, 1981; Haverkamp and Parlange, 1986; Nimmo et al., 2007; Arya et al., 2008). To obtain measurements over a range of ρ_2, each sand type was coated with different concentrations of an iron-oxide mineral, a process that is known to increase ρ_2 (Keating and Knight, 2007, 2012). We first present an analytical model for the relationship between the T_2-distribution and the VSD. Using the results from the laboratory experiments, we discussed the observed limitations

of this model. The results presented in this study comprise the first data set to systematically evaluate the effect of ρ_2 on the relationship between the T_2-distribution and the VSD. Understanding the effect of ρ_2 on this relationship is critical if NMR data are to be used to estimate the VSD in water-saturated geologic material.

BACKGROUND AND THEORY

An overview of the principles governing NMR theory is presented here; a more comprehensive discussion of NMR theory is presented in Coates et al. (1999) and Dunn et al. (2002). The NMR relaxation phenomenon is exhibited in nuclei with an odd number of protons or neutrons because these nuclei possess a spin angular momentum. In our research, the hydrogen atom with a single proton is of interest because of its presence in water. In a static magnetic field, the protons will align with and precess about the field resulting in a net magnetization proportional to the total number of protons in the sample. The NMR experiment starts when an oscillating magnetic field, tuned to detect protons in hydrogen, is applied to the sample for a short time causing the spins to tilt away from their initial alignment. Once the secondary pulse is removed, the protons relax back to their initial position resulting in a measurable decay of magnetization with time t. In this study, we focus on the transverse component of the NMR signal $I_{xy}(t)$ because this is the component of the signal most commonly measured in near-surface geophysical studies.

NMR relaxation assuming fast diffusion

$I_{xy}(t)$ is described by a multiple exponential decay,

$$I_{xy}(t) = I_0 \sum_i h_i e^{-t/T_{2i}}, \tag{1}$$

where h_i is the fraction of the signal relaxing with a relaxation time of T_{2i}. In NMR studies of geologic material, it is typically assumed that pores are isolated and that relaxation occurs in the fast diffusion regime in which case each component of the sum corresponds to a single-pore environment. The boundary of the fast diffusion regime is defined by the control parameter κ,

$$\kappa \equiv \frac{\rho_2 a}{D} \ll 1, \tag{2}$$

where ρ_2 is the surface relaxivity; a is the average distance that a proton must travel to reach a paramagnetic site — here paramagnetic indicates ions with an unpaired electron such as iron(III); and D is the self-diffusion coefficient ($D = 2.46 \times 10^{-9}$ m^2/s for water at 30°C). Ryu (2009) suggests that using the limit $\kappa < 0.1$ is a sufficient condition for determining if relaxation occurs in the fast diffusion regime.

The ith relaxation time is given by

$$\frac{1}{T_{2i}} = \frac{1}{T_{2Si}} + \frac{1}{T_{2B}} + \frac{1}{T_{2Di}}, \tag{3}$$

where T_{2Si} is the ith relaxation time; T_{2B} is the bulk fluid relaxation rate; T_{2Di} is the diffusion relaxation time; and T_{2B}^{-1}, T_{2Si}^{-1}, and T_{2Di}^{-1} are referred to as the bulk fluid, surface, and diffusion relaxation rates, respectively. The magnitude of T_{2B} is governed

by the viscosity of the pore water and the concentration of dissolved paramagnetic species, e.g., oxygen, $Mn^{2+}(aq)$, and $Fe^{3+}(aq)$ (Bloembergen et al., 1948; Bryar et al., 2000). The T_{2Di} value is affected by the inhomogeneities in the static magnetic field.

In geologic material, it is generally assumed that 1) surface relaxation is the dominant relaxation mechanism, i.e., $T_{2Si}^{-1} \gg T_{2B}^{-1}$, 2) relaxation occurs in the fast diffusion regime, 3) the surface relaxivity is constant across all pores, and 4) the inhomogeneities in the magnetic field are negligible, i.e., $T_{2D}^{-1} = 0$. In this case, the relaxation time in each pore can be expressed as

$$\frac{1}{T_{2i}} \sim \frac{1}{T_{2Si}} = \rho_2 \frac{\alpha}{r_{v-i}} = \rho_2 S_{\text{por}-i}, \qquad (4)$$

where r_{v-i} is the characteristic radius of the ith pore and α is a geometric factor, which is 1 for planar pores, 2 for cylindrical pores, and 3 for spherical pores. For ideal pore shapes, $\alpha/r_{v-i} = S_{\text{por}-i}$, where $S_{\text{por}-i}$ is the surface-area-to-volume ratio of the ith pore. Under these assumptions, the T_2-distribution is a linear transformation of the VSD (e.g., Hinedi et al., 1997). The surface relaxivity term in equations 2 and 4 has been shown experimentally to be related to the concentration and mineralogy of paramagnetic species on the surface of the pore (Foley et al., 1996; Bryar et al., 2000; Keating and Knight, 2007, 2010).

The mean log relaxation time T_{2ML} is often used to represent a single value for the relaxation time distribution and is calculated from the weighted geometric mean of the T_2-distribution,

$$\log T_{2ML} = \sum_i h_i \log T_{2i}. \qquad (5)$$

Equation 3 is then rewritten as

$$\frac{1}{T_{2ML}} = \frac{1}{T_{2S}} + \frac{1}{T_{2B}} + \frac{1}{T_{2D}}, \qquad (6)$$

where T_{2S} and T_{2D} are now the surface and diffusion relaxation times averaged over the entire pore space.

The diffusion relaxation time is calculated from (Kleinberg and Horsfield, 1990)

$$\frac{1}{T_{2D}} = \frac{D}{12}(\gamma G t_E)^2, \qquad (7)$$

where G is the average magnetic field gradient and t_E is the echo time, an NMR measurement parameter. The value of T_{2D}^{-1} can be determined by collecting NMR measurements at multiple values of t_E. If T_{2ML}^{-1} is constant with t_E^2, then the effect of magnetic field inhomogeneities is negligible.

NMR relaxation without assuming fast diffusion

Outside of the fast diffusion regime, the NMR signal in a single pore $I_{xy-i}(t)$ is described by a multiexponential decay (Brownstein and Tarr, 1979):

$$I_{xy-i}(t) = I_0 h_i \sum_k f_k e^{-t/T_{2Si-k}}, \qquad (8)$$

where $I_0 h_i$, from equation 1, is proportional to the number of protons in the pore and f_k is the relative amplitude of each component

of the magnetization decaying with a relaxation time of T_{2Si-k}. In equation 8, the diffusion and bulk fluid relaxation times have been neglected. The sum is arranged such that $T_{2Si-0} > T_{2Si-1} > T_{2Si-2} \ldots$, and the k term in the sum is referred to as the kth relaxation mode.

In the slow diffusion regime, defined by $\kappa \gg 10$, most of the relaxation ($>60\%$) occurs in the zeroth or slowest relaxation mode. In the intermediate diffusion regime, defined as $1 \ll \kappa \ll 10$, almost all of the relaxation occurs in the zeroth mode with only a few percent ($<5\%$) relaxing in the higher modes. For the slow and intermediate regimes, the amount of relaxation occurring in the zeroth mode depends on the characteristic shape of the pore. For the fast diffusion regime $f_k = 0$ for $k > 0$, the magnetization can be expressed as a single exponential decay. In all regimes, the zeroth mode relaxation time can be expressed as (Godefroy et al., 2001)

$$\frac{1}{T_{2Si-0}} = \frac{1}{\frac{r_{v-i}}{\alpha\rho_2} + \frac{r_{v-i}^2}{2\alpha D}}, \qquad (9)$$

where r_v is the characteristic pore radius and α is a factor that accounts for the geometry of the pore (α is 1 for planar pores, 2 for cylindrical pores, and 3 for a spherical pore). In the slow diffusion regime, the second term in the denominator of equation 9 dominates. In the fast diffusion limit, the first term in the denominator of equation 9 dominates and T_{2Si-0} can be expressed as in equation 4.

VSD and T_2-distribution

Our focus is the interpretation of T_2-distributions on materials with large pores and/or high ρ_2 in which the assumption of fast diffusion is violated. Using equation 9, we present an analytical model for the relationship between an idealized VSD and the corresponding T_2-distribution across a range of average pore radii, geometric factors, surface relaxivities, and VSD width. We represent the VSD using a lognormal distribution, i.e., $\log r_v \sim N(\mu_r, \sigma_r^2)$, where r_v is the characteristic pore radius, which is commonly used to represent the VSD for monomodal distributions of pore sizes (e.g., Nimmo, 1997; Hwang and Powers, 2003):

$$f(\log r_v; \mu_r, \sigma_r^2) = \frac{1}{\sigma_r\sqrt{2\pi}} e^{-\frac{1}{2}\left(\frac{\log r_v - \mu_r}{\sigma_r}\right)^2}. \qquad (10)$$

Here, μ_r is the weighted arithmetic mean of $\log r_v$ and σ_r^2 is the variance of $\log r_v$ and represents the width of the VSD. The value of μ_r is related to the weighted geometric mean pore radius by $r_{ML} = 10^{\mu_r}$.

Within the fast diffusion regime, each pore exhibits a single exponential decay, and, because the T_2-distribution is a linear transformation of the VSD, if $\log r_v$ is normally distributed, $\log T_2$ is also normally distributed. That is, $\log T_2 \sim N(\mu_{T2}, \sigma_{T2}^2)$, where μ_{T2} is the weighted arithmetic mean of $\log T_2$, i.e., $T_{2ML} = 10^{\mu r2}$ and σ_{T2}^2 is the variance of $\log T_2$. In this case, $T_{2ML} = r_{ML}/(\rho_2\alpha)$ and the width of T_2-distribution is the same as the width of the VSD; i.e., $\sigma_{T2}^2 = \sigma_r^2$.

Outside of the fast diffusion regime, the NMR signal from a single pore exhibits multiexponential decay; however, in our analytical model, we only focus on how the VSD affects the distribution of zeroth mode relaxation time values, we call this modified

T_2-distribution the T_{2-0}-distribution. Because in the intermediate and slow diffusion regime most of the NMR signal is in the zeroth mode, understanding how the T_{2-0}-distribution varies with the VSD corresponds to understanding how the largest peak, centered at long relaxation times, in the T_2-distribution varies as a function of the VSD. In the zeroth mode, the relaxation time of a pore is related to the radius of that pore by equation 9; this relationship implies that if log $r_v \sim N(\mu_r, \sigma_r^2)$ then log $T_{2-0} \sim N(\mu_{T2}, \sigma_{T2}^2)$, where μ_{T2} is the weighted arithmetic mean of log T_{2-0} and σ_{T2}^2 is the variance of log T_{2-0}. The mean log relaxation time of the T_{2-0}-distribution is $T_{2-0ML} = 10^{\mu_{r2}}$.

Figure 1 shows the plots of T_{2-0ML} as a function of κ (Figure 1a) and σ_{T2}^2, normalized by σ_r^2, as a function of κ (Figure 1b), where κ is used to represent changes with ρ_2 and is calculated from equation 9 using r_{ML}. Also shown in Figure 1 are the regions representing the fast, intermediate, and slow diffusion regimes. Because κ was calculated from r_{ML}, the regions in Figure 1 represent the relaxation

regime of pores of size equal to or less than r_{ML} and do not represent the relaxation regime for all pores.

The plot of T_{2-0ML} versus κ is shown in Figure 1a for a range of realistic pore sizes and geometries ($r_{ML} = 1$ and $100~\mu m$; $\alpha = 1$ and 10), as well as for narrow ($\sigma_r^2 = 0.01$) and broad ($\sigma_r^2 = 1$) VSDs. For the narrow VSD, the relationship between T_{2-0ML} and κ is the same as would be expected from a single pore; in the fast diffusion regime, T_{2-0ML} decreases with κ and in the slow diffusion regime T_{2-0ML} is constant with κ. For the broad VSD, there is a slight deviation in the relationship between T_{2-0ML} and κ from that of the narrow distribution. This deviation is primarily located in the intermediate relaxation regime where T_{2-0ML} is slower than for the narrow VSD; however, the deviation is small, and we do not anticipate that it will have a large impact on the interpretation of NMR data.

The normalized σ_{T2}^2 versus κ is shown in Figure 1b for the narrow ($\sigma_r^2 = 0.01$) and broad ($\sigma_r^2 = 1$) VSDs; the relationship is invariant of r_{ML} and α. For the narrow and broad VSD, the normalized σ_{T2}^2 is equal to one for small values of κ and increases with κ. The increase in normalized σ_{T2}^2 starts well before the fast diffusion limit, at $\kappa \sim 0.1$ for the narrow VSD and at $\kappa \sim 0.01$ for the broad VSD. This observation lends additional support for using $\kappa < 0.1$ as a sufficient condition for the assumption of fast diffusion. In the slow diffusion regime, the normalized σ_{T2}^2 reaches a maximum of four, indicating that, in log space, the T_2-distribution can be twice as wide as the VSD. The broadening of the T_{2-0}-distribution in the slow diffusion regime is in addition to the multiexponential relaxation that occurs in a single pore in this regime. Based on this analysis, we anticipate that, for samples near the upper limit or outside of the fast diffusion regime, the broadening of the T_2-distributions could lead to misinterpretation of NMR data.

MATERIALS AND METHODS

Material and sample preparation

We designed our experiment to determine the effect of ρ_2 on the relationship between the T_2-distribution and the VSD of water-saturated sands. Silica sand (99.5% SiO_2, 0.157% Al_2O_3, 0.084% Fe_2O_3; Best Sand Corporation) was used as an analog for a naturally occurring material in this study. We used three sands, each with a different range of grain sizes: a fine sand (mesh 100–270), a medium sand (mesh 70–100), and a coarse sand (mesh 20–40). To make materials with different ρ_2, we created subsets of each sand with different surface chemical properties. One subset was left uncoated, and two subsets were coated with different concentrations of the iron mineral hematite (Fe_2O_3) (low concentration and high concentration). Coating sand with hematite was expected to change the ρ_2 of the sand (Keating and Knight, 2007, 2012). This procedure resulted in nine sample sands: uncoated, low-coated, and high-coated fine sand; uncoated, low-coated, and high-coated medium sand; and uncoated, low-coated, and high-coated coarse sand.

Hematite was prepared and coated onto the surface of the sands using the procedure described in Keating and Knight (2007). Hematite was first synthesized by the forced hydrolysis of a Fe(III) salt solution (1 M $Fe(NO_3)_3$) (Schwertmann and Cornell, 2000). Once synthesized, the hematite slurry was filtered by dialysis to remove excess salts. The hematite slurry was then mixed with the silica sand and left to dry. Two different ratios of hematite slurry to silica sand
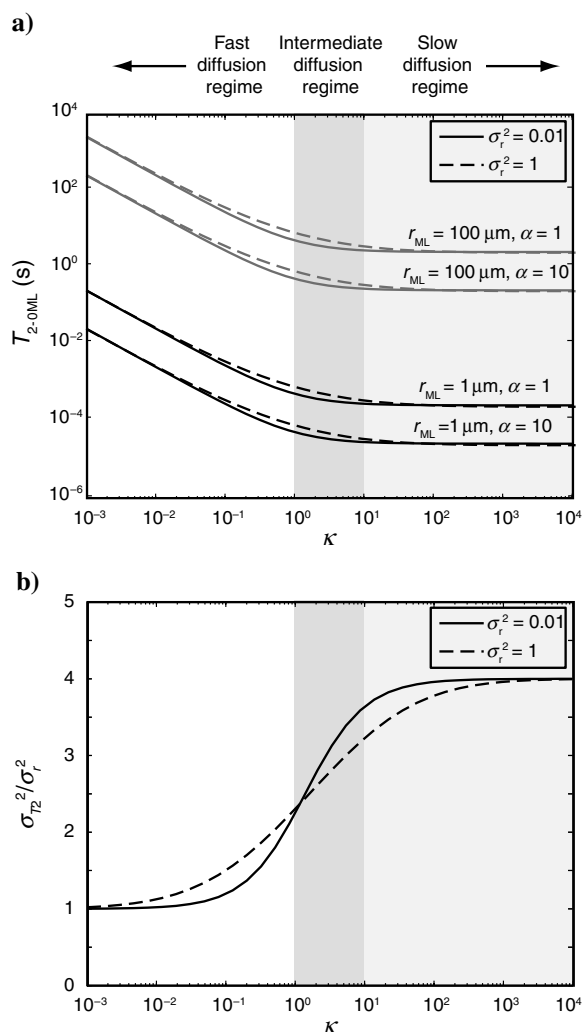
a)

b)

Figure 1. Theoretical relationship between the mean log relaxation time of the zeroth mode relaxation times T_{2-0ML} and the control parameter κ (a) and the normalized variance of the log T_{2-0} distribution and κ (b) for a variety of parameters affecting the VSD.

were used for each grain size to create the low- and high-coated sands.

Prior to NMR measurements, all coated and uncoated sands were washed to remove fine particulate matter and hematite not adhered to the sand surface. First, the coated and uncoated sands were washed by rinsing with distilled deionized water five or six times. The sands were then packed into a column and flushed with distilled deionized water at a flow rate of 0.1 mL/min for 48 hours. Once washed, the sands were dried in an oven at 80°C.

NMR measurements

Three samples, used for the NMR measurements, were made from each type of the washed sands. The first two NMR samples were created using the bulk washed sand. Due to limited materials, following NMR measurements on the first two samples, the sand from these samples was dried and mixed with the unused washed sand; this mixture was used to create a third NMR sample. To create an NMR sample, the sand was packed into a cylindrical Teflon sample holder (height, 56.3 mm; inner diameter, 31.0 mm). The lid of each sample holder was perforated with holes less than 0.1 mm in diameter. A filter (25 μm) was placed at the top of the sample to prevent sand grains from escaping the sample holder during the saturation process. Once packed, the samples were weighed to determine the dry sand mass.

Each sample was saturated by placing the sample, submerged in a beaker of distilled deionized water, in a vacuum chamber and reducing the pressure in the chamber to ~100 mmHg for 10 min. Air was then allowed to enter into the chamber until atmospheric pressure was reached; the pressure was then reduced a second time for 20 min. The volume of water saturating the sample was then determined gravimetrically. Once saturated and weighed, each sample holder was covered with Parafilm to prevent water from evaporating over the course of the NMR experiment.

NMR relaxation data were collected with a 2-MHz NMR Rock Core Analyzer (Magritek Ltd.) using a Carr-Purcell-Meiboom-Gill (CPMG) pulse sequence. Data were collected at echo times of 200, 400, 600, and 800 μs; 32 data points were obtained at each echo. The data were stacked 32 times; i.e., 32 data records were collected and averaged to improve the signal-to-noise ratio, and the number of echoes was chosen such that the total run time was 10 s per stack. Measurements were consistently made at 30°C to prevent changes in the NMR response of the sample due to variations in temperature.

To determine the T_2-distributions, the NMR data sets from the water-saturated sand samples were inverted using a nonnegative least-squares inversion routine with second-order Tikhonov regularization (Whittall et al., 1991). Prior to inverting the data, each NMR data set was logarithmically subsampled to 5000 data points to improve the speed of the fitting algorithm. The subsampled data were then fit to a distribution of 160 logarithmically spaced T_2 values ranging from 0.1 ms to 10 s. The regularization parameter for each fit was selected using the L-curve criteria.

Once the NMR data had been collected on a water-saturated sand sample, the pore water was removed by vacuum filtration using a 25-μm filter. An NMR measurement was made using pore water with the same parameters as for the water-saturated sand samples. The NMR data set from the extracted pore water was fit to a single exponential decay using a least-squares algorithm and used to obtain the bulk fluid relaxation time.

Material characterization

To characterize the chemical and physical properties of the sands, subsamples were collected from the washed sand and used for iron concentration, surface area, and grain size analysis. To ensure representative measurements, the bulk sand was thoroughly shaken prior to subsampling.

Three subsamples of 1 g each were used to determine the surface iron concentration. Each subsample was digested in 2 mL of hydrochloric acid (6 N) for approximately one week to dissolve all iron coated on the surface of the sand. The acid digest was then diluted (1:100), and the concentration of iron dissolved in the diluted solution was measured spectrophotometrically at 562 nm by means of the ferrozine method (Stookey, 1970).

Three subsamples of approximately 10 g each were used for surface area analysis. The specific surface area, defined as the surface area normalized by the sample mass, was measured for each subsample using the Brunauer-Emmett-Teller (BET) adsorption method with nitrogen gas $N_2(g)$ as the adsorbate. The measurements were collected with the Accelerated Surface Area and Porosimetry System (ASAP 2020, Micromeritics Instrument Corp.), which produces accurate results for samples with a total measured surface area greater than 1 m². For samples in which the total surface area was found to be less than 1 m² using N_2-BET, the measurements were verified by making a BET measurement on an additional subsample using krypton gas as the absorbate.

Three subsamples were used for grain-size analysis. To ensure accurate measurements, the amount of the subsample was increased until the total obscurance measured was between 9 and 13. The GSD was measured for each sample using a laser diffraction particle size analyzer (LS 13320, Beckman Coulter) with a 780-nm laser beam that is capable of measuring grains in the range of 0.4–2000 μm. This measurement provides a continuous GSD that is accurate for materials with low silt and clay content (Eshel et al., 2004). For each subsample, the measurement was repeated five times.

RESULTS

Chemical and physical properties

The experimentally determined chemical and physical properties are given in Table 1. The values given in Table 1 are the averages of the repeated measurements; the errors are the standard deviations.

The measured concentration of iron for each sand, as a percentage of grams of iron per grams of sand, is given in Table 1. The iron concentration ranged from 0.07% for the uncoated coarse sand to 0.38% for the high-coated fine sand. The iron concentration was nonzero for the uncoated sand because the sand used in this study is not pure silica. For the sands of the same grain sizes, the iron concentration was highest for the high-coated sand as expected. The iron concentration of the uncoated sand was slightly less than that of the low-coated sand for the medium and coarse sand; however, for the fine sands, the measured iron concentrations for the uncoated and the low-coated sand were the same within error. The small or negligible difference between the uncoated and low-coated sands is likely because the iron coating did not adhere to the surface of the sand and/or a larger than anticipated amount of iron was removed when the sand was washed.

The value of S_s ranged from 0.080 m²/g for the uncoated coarse sand to 0.55 m²/g for the high-coated fine sand. For the uncoated sand, the value of S_s decreased with grain size. The total surface area was less than 1 m² for the uncoated coarse sand; however, S_s determined from krypton BET measurement was 0.082 m²/g and confirmed the results shown in Table 1. For sands of the same grain size, the value of S_s increased with iron concentration. The larger values of S_s for the sands with higher concentrations of iron are consistent with previously published results (Keating and Knight, 2007, 2012).

The porosity ϕ was determined by dividing the gravimetrically determined volume of water in each sample by the total volume of the sample holder. For all samples, the values of ϕ, given in Table 1, fell in a narrow range from 0.40 ± 0.02 for the high-coated medium sand to 0.418 ± 0.006 for the uncoated fine sand. The porosity ϕ did not show a trend with iron concentration or with grain size.

For each NMR sample, S_{por} was calculated from S_s by

$$S_{por} = \frac{S_s m_s}{V_w}, \qquad (11)$$

where m_s is the mass of sand in the sample and V_w is the gravimetrically determined volume of water in a fully saturated sample. The value of S_{por}, shown in Table 1, ranged from 0.329 ± 0.005 μm⁻¹ for the uncoated coarse sand to 2.0 ± 0.1 μm⁻¹ for the high-coated fine sand. For all the sands, S_{por} increased with iron concentration.

GSD and average grain diameter

One GSD for each sand is shown in Figure 2; repeated measurements showed similar distributions. For all sands, the GSD is a single peak. The GSDs did not show a measurable dependence on iron concentration, indicating that the addition of the hematite coating did not result in a measurable change in grain size.

The mean log grain diameter d_{ML} was calculated from the GSD using the weighted-geometric mean:

$$\log d_{ML} = \sum_j h_j \log d_j, \qquad (12)$$

where h_j is the fraction of grains with a diameter of d_j and the sum is taken over the range of diameters measured. The values of d_{ML} are given in Table 1; the errors are the standard deviations across repeated measurements and samples. For the fine sands, d_{ML} ranged from 129 ± 11 to 139 ± 3 μm, for the medium sands, d_{ML} ranged from 235 ± 13 to 256 ± 2 μm, and for the coarse sand, d_{ML} ranged from 709 ± 33 to 753 ± 14 μm. The values of d_{ML} determined for the sands were within the expected range given the mesh sizes quoted by the manufacturer. As with the GSDs, the value of d_{ML} did not vary as a function of iron concentration.

Total initial signal intensity

Before considering the relaxation-time distributions, we first considered the volume of water detected in each sample by the NMR
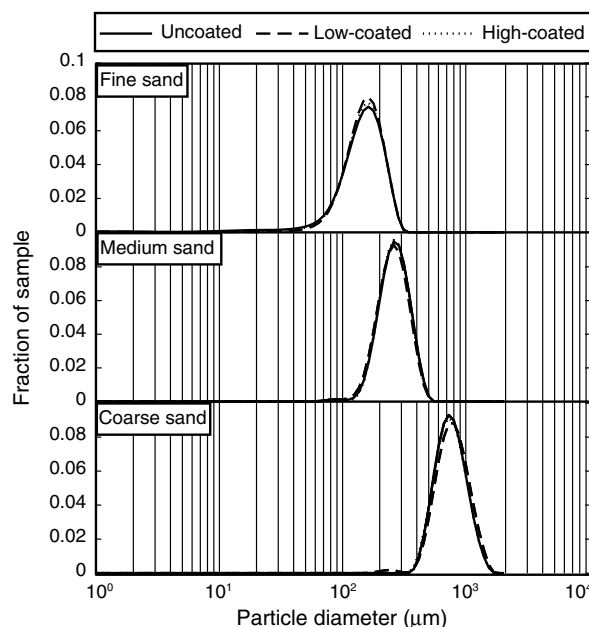

Figure 2. Experimentally determined GSDs.

Table 1. Experimentally determined physical properties.

Sample description		[Fe] (% g-Fe/g-sand)	S_s (m²/g)	ϕ	S_{por} (μm⁻¹)	d_{ML} (μm)
Grain size	Iron coating					
Fine	Uncoated	0.18 ± 0.04	0.37 ± 0.01	0.418 ± 0.006	1.36 ± 0.05	129 ± 11
	Low	0.18 ± 0.01	0.373 ± 0.003	0.414 ± 0.006	1.41 ± 0.03	139 ± 3
	High	0.38 ± 0.05	0.55 ± 0.02	0.42 ± 0.01	2.0 ± 0.1	135 ± 5
Medium	Uncoated	0.08 ± 0.01	0.15 ± 0.01	0.401 ± 0.008	0.58 ± 0.02	235 ± 13
	Low	0.09 ± 0.01	0.20 ± 0.02	0.415 ± 0.003	0.741 ± 0.004	238 ± 6
	High	0.20 ± 0.03	0.306 ± 0.009	0.40 ± 0.02	1.20 ± 0.06	256 ± 2
Coarse	Uncoated	0.07 ± 0.02	0.080 ± 0.007	0.392 ± 0.004	0.329 ± 0.005	733 ± 16
	Low	0.10 ± 0.02	0.120 ± 0.005	0.409 ± 0.002	0.462 ± 0.004	709 ± 33
	High	0.22 ± 0.05	0.224 ± 0.006	0.408 ± 0.009	0.86 ± 0.03	753 ± 14

Iron concentration, specific surface area S_s, porosity ϕ, pore-surface-area-to-volume ratio S_{por}, and mean grain diameter d_{ML}. Each value reported represents the average across repeated samples and/or measurements, and the errors are the standard deviation.

measurement. We are interested in the NMR-estimated water volume to determine if all the water within each measured sample is detected. The NMR-estimated water volume was calculated by multiplying the total signal intensity $I(0) = I_0$ by an instrument-specific calibration factor. The calibration factor is equal to the slope of I_0 versus V_w and was determined from NMR measurements collected on known volumes of distilled, deionized water. The NMR estimated volume of water versus V_w is shown in Figure 3; 1:1 correspondence is also plotted as a dashed line. From Figure 3, we see that the volume of water in each sample was accurately estimated from the NMR measurements and no signal loss was observed. The error ranges from 0.72% to 4.6% with an average error of 2.6%; these values are within the range previously found for laboratory CPMG measurements on water-saturated sandstone cores and sand packs (Peyron et al., 1996; Keating and Knight 2012).

Relaxation time distribution and mean log relaxation rate

Each NMR data set displayed a multiexponential decay of signal amplitude. The T_2-distributions at an echo time of 200 μs for one sample of each material type are shown in Figure 4; measurements on repeated samples showed similar results. The T_2-distributions represent the contribution from T_{2S} and T_{2B}. The T_2-distributions for the uncoated sands (solid lines in Figure 4) all showed a similar shape: one main peak centered at long relaxation times with smaller secondary peaks centered at shorter relaxation times. For the fine and medium sand, there was one distinct secondary peak, and for the coarse sand, there were two overlapping secondary peaks. For the coated sands, the peaks broadened and merged with increasing iron concentration. Similar trends have been observed for clean sand coated with iron minerals (Keating and Knight, 2007) and for mixtures of clean sand and hematite (Grunewald and Knight, 2011). There are two possible reasons for the presence of the smaller peaks centered at faster relaxation times: (1) There are small pores within the sand packs not captured by the laser particle size analysis and (2) these small peaks correspond to higher relaxation modes in the distributions due to relaxation occurring outside of the fast diffusion regime.

T_{2ML}^{-1} was calculated from the relaxation-time distributions using equation 5; the average values of the three repeated samples are given in Table 2. T_{2ML}^{-1} varied as a function of the grain size and iron concentration. For the uncoated sand, T_{2ML}^{-1} decreased with d_{ML}. For sands with similar values of d_{ML}, T_{2ML}^{-1} increased with iron concentration; however, for the coarse sand, the range of T_{2ML}^{-1} values was much smaller than the range for the medium sand.

Bulk fluid, diffusion, and surface relaxation rates

The values of the bulk fluid relaxation rate T_{2B}^{-1}, determined using a single exponential fit to the NMR data set on the extracted pore water from each sample, are shown as the white portion of each bar in Figure 5. All data shown were collected with an echo time of 200 μs and are an average of the data collected from three samples. Analysis of the residuals indicated that a single exponential decay was a valid assumption. Here, T_{2B}^{-1} exhibited a narrow range of values from 0.377 ± 0.08 s^{-1} for the high-coated medium sand to 0.4 ± 0.1 s^{-1} for the low-coated medium sand and showed no trend with grain size or iron concentration. For all samples, T_{2B}^{-1} was greater than the value of 0.328 s^{-1} previously reported for deionized water (Keating and Knight, 2007). The increase in T_{2B}^{-1} from that of deionized water is most likely because of the presence of dissolved paramagnetic species or suspended mineral particles within the pore water.

For each sample, the diffusion relaxation rate was determined as described by Keating and Knight (2007) by calculating the slope of the line fit to the plot of T_{2ML}^{-1} versus t_E^2. The slope was found to be zero within error for all measured samples, indicating that T_{2D}^{-1} was negligible. The same result was shown for hematite-coated sand in two previous studies (Keating and Knight, 2007, 2012). We note, however, for geologic material in which the characteristic pore size is small compared to the length scale over which a proton
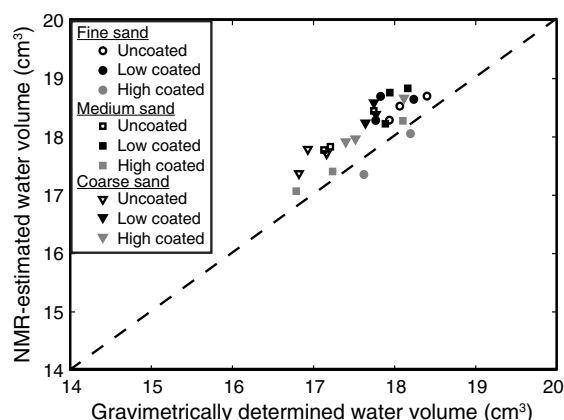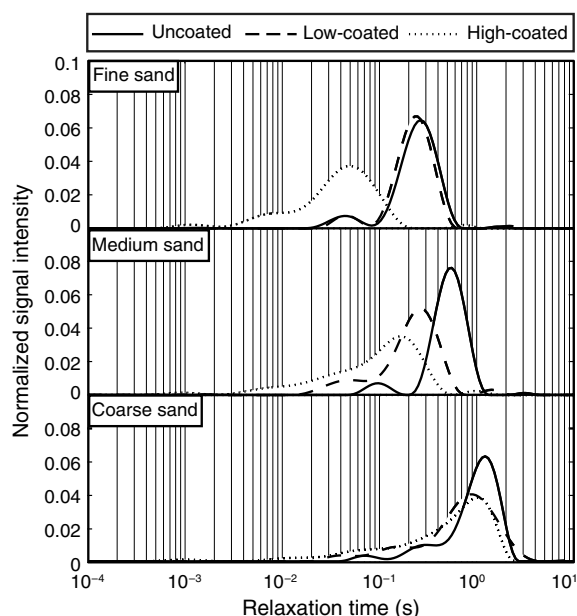
Figure 3. The gravimetrically determined volume of water versus the NMR-estimated water volume (the total signal intensity scaled by an experimentally determined calibration factor) for each measured sample. The dashed line represents equality.

Figure 4. Experimentally determined NMR relaxation time distributions obtained at an echo time of 200 μs. All distributions are normalized by the total signal amplitude.

dephases by 2π radians, it is possible that the relaxation rate would remain constant with t_E. To test for the effect of magnetic field inhomogeneities for the case of small pores, we use the collapsed data approach suggested by Hurlimann (1998) and find that the addition of hematite to the samples does not increase the effect of the magnetic field inhomogeneities.

The value of T_{2S}^{-1} was determined from the calculated values of T_{2ML}^{-1} and T_{2B}^{-1} measured at an echo time of 200 µs using equation 6. The calculated values of T_{2S}^{-1} are plotted for each sample at an echo time of 200 µs as the gray portion of each bar in Figure 5. From Figure 5, it is clear that surface relaxation was the dominant relaxation mechanism in all the samples measured in this study; i.e., $T_{2S}^{-1} > T_{2B}^{-1}$. As with T_{2ML}^{-1}, T_{2S}^{-1} varied as a function of grain size and iron concentration. For the uncoated sand, T_{2S}^{-1} decreased with grain size. For sands with similar values of d_{ML}, T_{2S}^{-1} increased with iron concentration.

Surface relaxivity

Because we expect that relaxation does not occur in the fast diffusion regime for the measured samples, equation 4 cannot be used to calculate ρ_2. Instead, we calculated ρ_2, assuming a spatially homogeneous value, from equation 9 by substituting S_{por} for α/r_v, where T_{2S} is an average across the entire pores space. We chose a value for α of 3, which corresponds to spherical pores. The average value of ρ_2 for each material type is given in Table 2; the errors are the standard deviation of ρ_2 calculated across the repeated samples. For the uncoated material, ρ_2 ranged from 2.34 ± 0.08 µm/s for the coarse sand to 3.20 ± 0.05 µm/s for the fine sand and showed a small increase with grain size. These values are consistent with previously published results where ρ_2 for silica sand ranged from 2.85 to 3.07 µm/s (Hinedi et al., 1997). For the fine and medium sand, ρ_2 increased with iron concentration; this observation is consistent with a previous study where ρ_2 increased with the concentration of paramagnetic ions (iron and manganese) doped to the surface of calcium silicates (Foley et al., 1996). However, for the coarse sand, ρ_2 did not show an increase with iron concentration and only exhibited a small range of values from

2.34 ± 0.08 µm/s for the uncoated material to 2.82 ± 0.08 µm/s for the low-coated material. We note that, as suggested by equation 9, an alternative method for calculating ρ_2 would be to assume a characteristic pore shape (i.e., spherical pores) and to use the average pore radius, estimated from the grain diameter, with the appropriate value of α. However, in a recent study performed by our laboratory, we found that for water-saturated glass beads, S_{por} was a better predictor of the surface relaxation time than the average grain radius and thus we have used S_{por} to calculate ρ_2 (Keating, 2013).

DISCUSSION

Diffusion regimes

To evaluate the diffusion relaxation regime for each sample, we calculated the control parameter κ using equation 2. If $\kappa < 0.1$, then the relaxation occurred in the fast diffusion. In equation 2, D is the self-diffusion coefficient of free water at 30°C, $D = 2.46 \times 10^{-9}$ m^2/s. We previously defined a as the average distance that a proton must travel to reach a paramagnetic site; for an ideal pore, a is equal to the pore radius. However, because for the samples in this study the value of a is unknown, we calculate two values of a: a
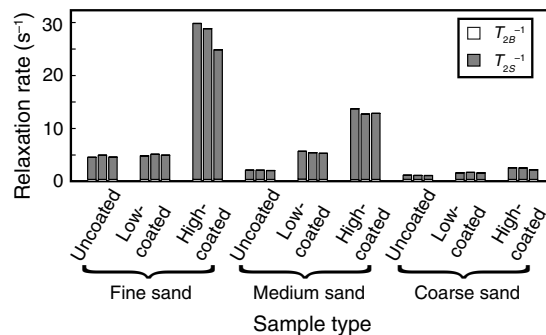

Figure 5. Stacked bar graph showing the experimentally determined NMR relaxation rates at an echo time of 200 µs; T_{2ML}^{-1} (length of the bar), T_{2B}^{-1} (white bar), and T_{2S}^{-1} (gray bar).

Table 2. Experimentally determined NMR parameters.

Sample description		T_{2ML}^{-1} (s^{-1})	ρ_2 (µm/s)	a_{low} (µm)	a_{up} (µm)	κ_{low}	κ_{up}
Grain size	Iron coating						
Fine	Uncoated	4.7 ± 0.2	3.20 ± 0.05	2.21	47	0.003	0.06
	Low	5.0 ± 0.5	3.28 ± 0.05	2.12	51	0.003	0.07
	High	28 ± 3	14.0 ± 0.6	1.49	49	0.008	0.27
Medium	Uncoated	2.11 ± 0.03	3.03 ± 0.05	5.2	86	0.006	0.1
	Low	5.5 ± 0.2	7.1 ± 0.2	4.05	87	0.011	0.24
	High	13.1 ± 0.5	10.9 ± 0.5	2.5	94	0.011	0.4
Coarse	Uncoated	1.15 ± 0.02	2.34 ± 0.08	9.1	268	0.009	0.25
	Low	1.66 ± 0.05	2.82 ± 0.08	6.49	259	0.007	0.29
	High	2.4 ± 0.2	2.4 ± 0.2	3.5	276	0.003	0.27

Mean log relaxation rate T_{2ML}^{-1}, the surface relaxivity ρ_2, the lower bound on the pore radius a_{low}, estimated from $a_{low} = \alpha/S_{por}$ assuming spherical pores (i.e., $\alpha = 3$), the upper bound on the pore radius a_{up} estimated from the largest sphere that can be inscribed in a simple cubic packing of spheres with diameters of d_{ML}, the lower bound on the control parameter κ_{low}, and the upper bound on the control parameter κ_{up}. Each value reported represents the average across repeated samples, and the errors are the standard deviation.

lower bound on the pore radius, which we call a_{low}, calculated from $S_{por} = 3/a_{low}$, and an upper bound on the pore radius, which we call a_{up}, calculated following the approach of Keating and Knight (2010) by estimating a_{up} from the largest sphere that can be inscribed in a simple cubic packing of spheres with diameters of d_{ML} (Gupta and Larson, 1979). We also calculate two corresponding values for κ: κ_{low}, which represents the lower bound on the control parameter, and κ_{up}, which represents the upper bound on the control parameter.

The values for a_{low} and κ_{low} are given in Table 2. For each grain size, the values for a_{low} range from 1.49 to 2.21 µm for the fine sand, from 2.5 to 5.2 µm for the medium sand, and from 3.5 to 9.1 µm for the coarse sand. Two observations are made from the values of a_{low}: 1) The values of a_{low} are almost two orders of magnitude smaller than the average grain size for each of the corresponding sands, which is much smaller than would be expected for grains of this size. 2) The values for a_{low} vary with the iron content, which is not expected given that the measured GSDs do not vary with the hematite coating. The corresponding values of κ_{low} are less than 0.1 for all sands; this indicates that relaxation could occur in the fast diffusion regime for the sands.

The values for a_{up} and κ_{up} are given in Table 2. The values for a_{up} ranged from 47 to 51 µm for the fine sand, 86 to 94 µm for the medium sand, and 259 to 276 µm for the coarse sand. The values of κ_{up} were less than 0.1 for the fine uncoated and low-coated sands, indicating that relaxation occurred in the fast diffusion regime for these samples. However, for the fine high-coated sands, the medium- and the coarse-grain sands κ_{up} was greater than 0.1, indicating that relaxation could occur outside the fast diffusion regime for these samples.

Comparison of GSDs to T_2-distributions

For all the sands, despite having similar GSDs and thus similar expected VSDs, the uncoated, low-coated, and high-coated sands have very different T_2-distributions (Figure 4). The location of the primary peak and the width of the T_2-distribution depend on the value of ρ_2. To quantify and compare the width of the T_2-distributions to the GSDs, the full-width at half-maximum (FWHM)

Table 3. The FWHM values for the grain size distributions FWHM$_{GSD}$, the relaxation time distributions FWHM$_{T_2}$, and the NMR-estimated VSDs FWHM$_{est-VSD}$.

Sample description				
Grain size	Iron coating	FWHM$_{GSD}$	FWHM$_{T_2}$	FWHM$_{est-VSD}$
Fine	Uncoated	0.4051	0.4717	0.4709
	Low	0.3808	0.4612	0.4605
	High	0.4051	0.6709	0.6706
Medium	Uncoated	0.3511	0.4088	0.4074
	Low	0.3511	0.5031	0.5024
	High	0.3241	0.7966	0.7960
Coarse	Uncoated	0.3592	0.4403	0.4370
	Low	0.3646	0.6289	0.6252
	High	0.3646	0.6604	0.6569

values were calculated and are given in Table 3. Comparing these values, we find that the sands with larger values of ρ_2 have broader T_2-distributions than samples with small values of ρ_2. Additionally, we find that the T_2-distributions are broader than the GSDs. These experimental results are consistent with our analytical observation that the T_2-distribution will be broader when relaxation does not necessarily occur in the fast diffusion regime. For these sands, assuming a linear relationship between the T_2-distribution and the VSD would clearly lead to inaccurate estimates of the VSD.

To compare the VSD to the T_2-distribution without assuming fast diffusion, we first transform each GSD into a VSD. Nimmo (1997) suggests that the ratio of the pore radius to the grain radius is approximately $(\phi/[1 - \phi])^{1/3}$, which yields a ratio of ~0.8 for the samples in this study. The VSD calculated from the GSD is shown in Figure 6.

We next transform each T_2 value to an equivalent pore radius using equation 9. Rearranging this equation to solve for r_v in terms of T_2 gives

$$r_v = \left(2\alpha D T_2 + \frac{D^2}{\rho_2^2}\right)^{1/2} - \frac{D}{\rho_2}. \qquad (13)$$

Using $\alpha = 3$, $D = 2.46 \times 10^{-9}$ m^2/s, and the value of ρ_2 for each sample (Table 2), we calculate an NMR-estimated VSD for each sample. The full methodology used to transform the T_2-distribution is outlined in Figure 7.

A representative NMR-estimated VSD for each material is shown along with a representative VSD for one sample of each grain size (plotted in terms of pore radius) in Figure 6. The FWHM values for the NMR-estimated VSDs are given in Table 3. From Figure 6 and Table 3, we see that this approach for estimating the VSD from the
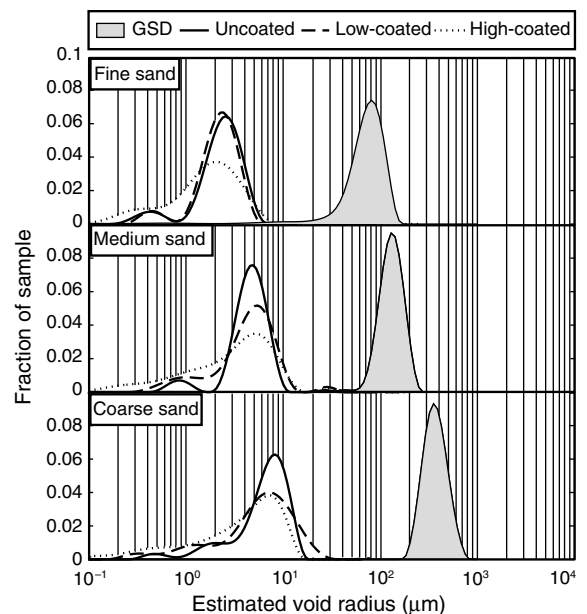

Figure 6. VSDs estimated from the NMR relaxation time distributions. Also shown for reference on each graph is the VSD, estimated from the grain size distribution, plotted as a function of pore radius for each sand.

T_2-distribution has yielded VSDs that are aligned with respect to each other. Although it was expected, as shown in Figure 1b, that the width of the estimated VSD would be narrower than the width of the T_2-distribution, the estimated VSDs are only slightly narrower than the original T_2-distribution with less than 0.6% difference between the FWHMs. As noted by the bounds of κ, relaxation for all samples could have occurred in the fast diffusion regime, which would explain the small difference in the width of the peaks. Another possible explanation for the small difference in the width of the peaks is that an incorrect value of α was used (i.e., the pores are not spherical); increasing the value of α increases the difference in the width of the T_2-distributions and the estimated VSDs. We also note that the peaks of the NMR-estimated VSDs are not aligned with the GSD and the NMR-estimated VSDs remain broader than the GSD. We conclude that this approach for estimating the VSD from the T_2-distribution is useful for understanding relative VSDs but fails to give an absolute measure of the true VSD.

Experimental methods and limitations

Several assumptions have been made in our approach that must be considered to determine if they explain the difference between the theoretical prediction that the NMR-estimated VSD would be narrower than the T_2-distribution and the observed difference between the NMR-estimated VSD and the GSDs. First, we have assumed that the value of ρ_2 is homogeneous across all surfaces; i.e., the hematite coating is uniform across all surfaces. Second, we have assumed that the surface area relevant for NMR measurements is the surface area determined from N_2-BET measurements. Finally, in our estimate of ρ_2, we have assumed that the pores can be represented by spheres; that is, $\alpha = 3$. In this section, we will evaluate these assumptions.

To evaluate the first assumption, that ρ_2 is homogeneous across all surfaces, we note that ρ_2 can be considered homogeneous as long as the distance between two paramagnetic sites is small relative to the distance that a proton can travel within the time scale of an NMR measurement. We can test this assumption by comparing the distance between two paramagnetic sites to the distance that a proton can diffuse before relaxing, ℓ_D. We expect that there are more than two paramagnetic sites in each pore, and so we obtain an upper limit

on the distance between two paramagnetic sites of a_{up}, where a_{up}, as previously defined in Table 2, is the average distance a proton needs to travel to reach a paramagnetic site. The value of ℓ_D is calculated from Einstein's equation for self-diffusion $\ell_D = \sqrt{6DT}$, where T is the relaxation time. If $a_{up} < \ell_D$, then our assumption is valid. Using the relaxation time for bulk fluid yielded a value for ℓ_D of approximately 190 μm. For the samples in this study, a_{up} is less than ℓ_D for the fine and medium sands but is greater than ℓ_D for the coarse sand. It is thus possible that spatial variability in ρ_2 could lead to a broadening of the relaxation time distribution (Keating and Knight, 2012); however, because a_{up} is only greater than ℓ_D for the coarse sands, and yet this behavior is observed in all sand samples, it is unlikely that spatial variability in ρ_2 explains the broad NMR-estimated VSDs determined in our study.

In our analysis, we have assumed that the surface area relevant for NMR measurements is the surface area determined from N_2-BET measurements. A corollary of this assumption is that the pore radius can be estimated from the measured value of S_{por} (i.e., a_{low} in Table 2). Although the N_2-BET measurement is commonly used to determine the surface area of unconsolidated materials, it provides a measure of the area available for nitrogen absorption and not the area relevant for NMR studies — that of the water-wetted surface. Differences between the VSD and the T_2-distribution in previous studies have been explained by suggesting that the N_2-BET measurement overestimated the water-wetted surface area. Similarly, in this study, we see that the radii determined from S_{por} (a_{low} in Table 2) are much smaller than the radii estimated from the GSD (a_{up} in Table 2). Overestimating the surface area would lead to underestimating the ρ_2, and so provides one possible explanation for the difference between the NMR-estimated VSD and the measured GSDs (e.g., Hinedi et al., 1997). However, at this time, there is no conclusive evidence showing that the N_2-BET measurement overestimates the area relevant for NMR measurements and, in fact, one study suggests that N_2-BET measurements actually underestimate the water-wetted surface area (Sokołowska et al., 2002). An alternative method for determining the value of ρ_2 would be to use the average pore radius, estimated from the grain radius; because α/r_v is less than S_{por}, this would result in a higher value for ρ_2. However, in a recent study from our laboratory, it was shown that for water-saturated glass bead packs, S_{por} is a better predictor of T_{2S} than r_v (as estimated from the grain diameter by assuming that the volume occupied by pores goes as the cube of r_v and that the volume occupied by the grains goes as the cube of d_{ML}; K. Keating, personal communication, 2013) and so in this study, we have chosen to use S_{por}.

An additional factor that may influence the NMR-estimated VSDs is the choice of the value α. In our estimate of ρ_2, we have chosen to use $\alpha = 3$, a value that corresponds to spherical pores. However, the true nature of the pores within the sand pack is likely not spherical. Recalculating the value of ρ_2 and the NMR-estimated VSD according to the flowchart in Figure 7, we find that using a value for α of ~100 yields NMR-estimated VSDs that are of the correct order of magnitude. However, if we consider realistic pore shapes, this value of α is much higher than expected. For example, assuming regular tetrahedral pores where the radius is one-half the length of one side, we find that $\alpha = 30$, which is less than needed to explain the discrepancy between the NMR-estimated VSD and the measured VSD. One possible explanation for this large value of α needed to correct the NMR-estimated VSD is that the pore surfaces

Collect raw NMR data

Invert for T_2-distribution

Calculate T_{2ML}

Calculate T_{2S} from $T_{2S}^{-1} = T_{2ML}^{-1} - T_{2B}^{-1}$

Calculate ρ_2 from $\rho_2 = (T_{2S}S_{por} + \alpha/(2DS_{por}))^{-1}$

Calculate κ from $\kappa = a\rho_2/D$

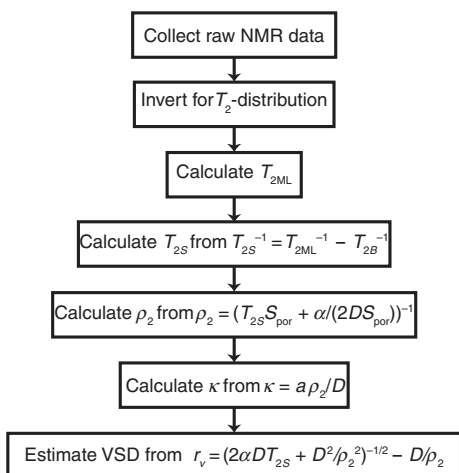Estimate VSD from $r_v = (2\alpha D T_{2S} + D^2/\rho_2^2)^{-1/2} - D/\rho_2$

Figure 7. Flowchart outlining the steps used to determine the NMR-estimated VSD from the T_2-distribution.

have fractal characteristics; however, more research is necessary to determine if the fractal nature of the pore surfaces can account for the discrepancy.

CONCLUSIONS

We have presented an analytical approach for obtaining an estimate of the VSD from the NMR relaxation time distribution and compared this approach to laboratory measurements on water-saturated sand packs. The analytical results show that estimating the VSD from the T_2-distribution assuming fast diffusion could lead to misinterpretation of NMR data. Specifically, for porous media in which relaxation occurs in the slow or intermediate diffusion regime, the T_2-distribution can be up to twice as broad as the true VSD. Our experimental results show that in fine to coarse sands with a range of surface relaxivities, the T_2-distributions are broader than the measured GSDs and are not centered around a single T_2 value. Using a general equation, which does not assume fast diffusion, to transform the T_2 values to pore radii yields NMR-estimated VSDs that were centered around a single pore radii. However, our attempts to recover the true VSD were unsuccessful; the NMR-estimated VSDs were broader and yielded average pore radii that were much smaller than expected. We conclude that while the approach outlined here is useful for determining relative VSDs, additional research is needed to improve our understanding of the link between the T_2-distribution and the VSD for unconsolidated sands. Continued research to refine this relationship will ultimately help to improve the interpretation of NMR measurements made on near-surface geologic material.

ACKNOWLEDGMENTS

REFERENCES

Allen, D., C. Flaum, T. S. Ramakrishnan, J. Bedford, K. Castelijns, D. Fairhurst, G. Gubelin, N. Heaton, C. C. Minh, and M. A. Norville, 2000, Trends in NMR logging: Oilfield Review, **12**, 2–19.

Arns, C. H., 2004, A comparison of pore size distributions derived by NMR and X-ray-CT techniques: Physica A, **339**, 159–165, doi: 10.1016/j.physa.2004.03.033.

Arya, L. M., D. C. Bowman, B. B. Thapa, and D. K. Cassel, 2008, Scaling soil water characteristics of golf course and athletic field sands from particle-size distribution: Soil Science Society of America Journal, **72**, 25–32; doi: 10.2136/sssaj2006.0232.

Arya, L. M., and J. F. Paris, 1981, A physicoempirical model to predict the soil moisture characteristic from particle-size distribution and bulk density data: Soil Science Society of America Journal, **45**, 1023–1030, doi: 10.2136/sssaj1981.03615995004500060004x.

Bird, N. R. A., A. R. Preston, E. W. Randall, W. R. Whalley, and A. P. Whitmore, 2005, Measurement of the size distribution of water-filled pores at different matric potentials by stray field nuclear magnetic resonance: European Journal of Soil Science, **56**, 135–143, doi: 10.1111/j.1351-0754.2004.00658.x.

Bloembergen, N., E. M. Purcell, and R. V. Pound, 1948, Relaxation effects in nuclear magnetic resonance absorption: Physical Review A, **73**, 679–712, doi: 10.1103/PhysRev.73.679.

Brownstein, K. R., and C. E. Tarr, 1979, Importance of classical diffusion in NMR studies of water in biological cells: Physical Review A, **19**, 2446–2453, doi: 10.1103/PhysRevA.19.2446.

Bryar, T. R., C. J. Daughney, and R. Knight, 2000, Paramagnetic effects of iron(III) species on nuclear magnetic relaxation of fluid protons in porous media: Journal of Magnetic Resonance, **142**, 74–85, doi: 10.1006/jmre.1999.1917.

Coates, G. R., L. Xioa, and M. G. Prammer, 1999, NMR logging principles and applications: Halliburton Energy Services.

Costabel, S., and U. Yaramanci, 2011a, Relative hydraulic conductivity in the vadose zone from magnetic resonance sounding — Brooks-Corey parameterization of the capillary fringe: Geophysics, **76**, no. 3, G61–G71, doi: 10.1190/1.3552688.

Costabel, S., and U. Yaramanci, 2011b, Relative hydraulic conductivity and effective saturation from earth's field nuclear magnetic resonance – A method for assessing the vadose zone: Near Surface Geophysics, **9**, 155–167, doi: 10.3997/1873-0604.2010055.

Costabel, S., and U. Yaramanci, 2013, Estimation of water retention parameters from nuclear magnetic resonance relaxation time distribution: Water Resources Research, **49**, 2068–2079, doi: 10.1002/wrcr.20207.

Dlugosch, R., M. Mueller-Petke, T. Gunther, S. Costabel, and U. Yaramanci, 2011, Assessment of the potential of a new generation of surface nuclear magnetic resonance instruments: Near Surface Geophysics, **9**, 89–102, doi: 10.3997/1873-0604.2010063..

Dunn, K. J., D. J. Bergmann, and G. A. LaTorraca, 2002, Nuclear magnetic resonance: Petrophysical and logging applications: Handbook of geophysical exploration: Pergamon.

Eshel, G., G. J. Levy, U. Mingelgrin, and M. J. Singer, 2004, Critical evaluation of the use of laser diffraction for particle-size distribution analysis: Soil Science Society of America Journal, **68**, 736–743, doi: 10.2136/sssaj2004.0736.

Foley, I., S. A. Farooqui , and R. Kleinberg, 1996, Effect of paramagnetic ions on NMR relaxation of fluids at solid surfaces: Journal of Magnetic Resonance, **123**, 95–104, doi: 10.1006/jmra.1996.0218.

Godefroy, S., J. P. Korb, M. Fleury, and R. G. Bryant, 2001, Surface nuclear magnetic relaxation and dynamics of water and oil in macroporous media: Physical Review E, **64**, 021605, doi: 10.1103/PhysRevE.64.021605.

Grunewald, E., and R. Knight, 2011, A laboratory study of NMR relaxation times in unconsolidated heterogeneous sediments: Geophysics, **76**, no. 4, G73–G83, doi: 10.1190/1.3581094.

Gupta, S. C., and W. E. Larson, 1979, Model for predicting packing density of soils using particle-size distribution: Soil Science Society of America Journal, **43**, 758–764, doi: 10.2136/sssaj1979.03615995004300040028x.

Haverkamp, R., and J. Y. Parlange, 1986, Predicting the water-retention curve from particle-size distribution — 1. Sandy soils without organic matter: Soil Science, **142**, 325–339, doi: 10.1097/00010694-198612000-00001.

Hinedi, Z. R., A. C. Chang, M. A. Anderson, and D. B. Borchardt, 1997, Quantification of microporosity by nuclear magnetic resonance relaxation of water imbibed in porous media: Water Resources Research, **33**, 2697–2704, doi: 10.1029/97WR02408.

Hinedi, Z. R., Z. J. Kabala, T. H. Skaggs, D. B. Borchardt, R. W. K. Lee, and A. C. Chang, 1993, Probing soil and aquifer material porosity with nuclear magnetic resonance: Water Resources Research, **29**, 3861–3866, doi: 10.1029/93WR02302.

Hurlimann, M. D., 1998, Effective gradients in porous media due to susceptibility differences: Journal of Magnetic Resonance, **131**, 232–240, doi: 10.1006/jmre.1998.1364.

Hwang, S. I., and S. E. Powers, 2003, Lognormal distribution model for estimating soil water retention curves for sandy soils: Soil Science, **168**, 156–166, doi: 10.1097/01.ss.0000058888.60072.e3.

Keating, K., and R. Knight, 2007, A laboratory study to determine the effect of iron oxides on proton NMR measurements: Geophysics, **72**, no. 1, E27–E32, doi: 10.1190/1.2399445.

Keating, K., and R. Knight, 2010, A laboratory study of the effect of Fe(II)-bearing minerals on nuclear magnetic resonance (NMR) relaxation measurements: Geophysics, **75**, no. 3, F71–F82, doi: 10.1190/1.3386573.

Keating, K., and R. Knight, 2012, The effect of spatial variation in surface relaxivity on nuclear magnetic resonance relaxation rates: Geophysics, **77**, no. 5, E365–E377, doi: 10.1190/geo2011-0462.1.

Kleinberg, R., and M. A. Horsfield, 1990, Transverse relaxation processes in porous sedimentary rock: Journal of Magnetic Resonance, **88**, 9–19, doi: 10.1016/0022-2364(90)90104-H.

Kleinberg, R. L., 1994, Pore size distributions, pore coupling, and transverse relaxation spectra of porous rocks: Magnetic Resonance Imaging, **12**, 271–274, doi: 10.1016/0730-725X(94)91534-2.

Legchenko, A., J. M. Baltassat, A. Bobachev, C. Martin, H. Robain, and J. M. Vouillamoz, 2004, Magnetic resonance sounding applied to aquifer characterization: Ground Water, **42**, 363–373, doi: 10.1111/j.1745-6584.2004.tb02684.x.

Nimmo, J. R., 1997, Modeling structural influences on soil water retention: Soil Science Society of America Journal, **61**, 712–719, doi: 10.2136/sssaj1997.03615995006100030002x.

Nimmo, J. R., W. N. Herkelrath, and A. M. Laguna Luna, 2007, Physically based estimation of soil water retention from textural data: General framework, new models, and streamlined existing models: Vadose Zone Journal, **6**, 766–773, doi: 10.2136/vzj2007.0019.

Peyron, M., G. K. Pierons, H. J. Lucas, L. D. Hall, and R. C. Stewart, 1996, The modified stretched-exponential model for characterization of NMR relaxation in porous media: Journal of Magnetic Resonance, **118**, 214–220, doi: 10.1006/jmra.1996.0029.

Ryu, S., 2009, Effect of inhomogeneous surface relaxivity, pore geometry and internal field gradients on NMR logging: Exact and perturbative theories and numerical investigations: Presented at Society of Petrophysicists and Well Log Analysts 50th Annual Logging Symposium.

Schaumann, G. E., E. Hobley, J. Hurrass, and W. Rotard, 2005, H-NMR relaxometry to monitor wetting and swelling kinetics in high-organic matter soils: Plant and Soil, **275**, 1–20, doi: 10.1007/s11104-005-1708-7.

Schwertmann, U., and R. M. Cornell, 2000, Iron oxides in the laboratory: Wiley-VCH.

Sokołowska, Z., M. Borówko, J. Reszko-Zygmunt, and S. Sokołowski, 2002, Adsorption of nitrogen and water vapor by alluvial soils: Geoderma, **107**, 33–54, doi: 10.1016/S0016-7061(01)00137-9.

Stookey, L. L., 1970, Ferrozine — A new spectrophotometric reagent for iron: Analytical Chemistry, **42**, 779–781, doi: 10.1021/ac60289a016.

Straley, C., A. Matteson, S. Feng, L. M. Schwartz, W. E. Kenyon, and J. R. Banavar, 1987, Magnetic resonance, digital image analysis, and permeability of porous media: Applied Physics Letters, **51**, 1146–1148, doi: 10.1063/1.98766.

Straley, C., D. Roosini, H. J. Vinegar, P. Tutunjian, and C. E. Morriss, 1997, Core analysis by low-field NMR: The Log Analyst, **38**, 84–94.

Swanson, R. D., K. Singha, F. D. Day-Lewis, A. Binley, K. Keating, and R. Haggerty, 2012, Direct geoelectrical evidence of mass transfer at the laboratory scale: Water Resources Research, **48**, W10543, doi: 10.1029/2012WR012431.

Valckenborg, R., L. Pel, and K. Kopinga, 2001, Cryoporometry and relaxometry of water in silica-gels: Magnetic Resonance Imaging, **19**, 489–491, doi: 10.1016/S0730-725X(01)00275-2.

Walsh, D. O., E. Grunewald, P. Turner, and I. Frid, 2010, Javelin: A slimhole and microhole NMR logging tool: FastTimes, **15**, no. 3, 67–72.

Weller, A., S. Nordsiek, and W. Debschutz, 2010, Estimating permeability of sandstone samples by nuclear magnetic resonance and spectral-induced polarization: Geophysics, **75**, no. 6, E215–E226, doi: 10.1190/1.3507304.

Whittall, K. P., M. J. Bronskill, and R. M. Henkelman, 1991, Investigation of analysis techniques for complicated NMR relaxation data: Journal of Magnetic Resonance, **95**, 221–234, doi: 10.1016/0022-2364(91)90213-D.